Crazing in Glassy Block Copolymer Thin Films

Jong-Young Lee and Alfred J. Crosby*

Polymer Science and Engineering Department, University of Massachusetts, Amherst, Massachusetts 01003

Received August 2, 2005; Revised Manuscript Received September 14, 2005

ABSTRACT: We investigate the crazing process (craze initiation, growth, and failure) in symmetric polystyrene-*b*-poly(2-vinylpyridine) (PS-*b*-P2VP) glassy thin films. PS-*b*-P2VP is a model material for this study due to its ability to self-assemble into well-aligned lamellar microdomains and the similar mechanical properties for each block (glass transition temperature, crazing stress, entanglement molecular weight, and elastic modulus). These attributes allow us to focus on two primary effects: the effect of an ordered microstructure and the effect of surface terraces on the crazing process in thin glassy polymer films. We find that an ordered lamellar microstructure leads to a higher ratio of craze depth to film thickness in the micronecking process and a lower craze growth rate compared with polystyrene homopolymer. Additionally, surface terracing, or nanoscale steps in the surface topography, impedes craze initiation and significantly decreases the failure strain compared with polystyrene and PS-*b*-P2VP thin films without surface terraces. These results demonstrate the importance of nanoscale morphologies on the crazing process and point to new directions for understanding the fundamental mechanisms for crazing in advanced materials.

Introduction

Crazing is a localized deformation process which often leads to complete fracture or failure for many polymer materials. Prior to fracture, crazes themselves are detrimental to not only structural integrity but also many other properties, such as the local dielectric constant of a material. For this reason, crazing impacts numerous applications ranging from structural supports to electronic packaging. Crazing in homopolymers[1−9] and block copolymers[10−15] has been studied extensively over the past several decades. For block copolymers in particular, much of previous research has focused on rubber−glassy systems[10−14] (e.g., polystyrene-*b*-polybutadiene), where enhanced toughness can be achieved. In these materials, crazes grow by cavitation of rubber domains and elongation of voids, which is different from the conventional crazing mechanism and complicates analysis of block copolymer architecture on crazing. In glassy block copolymer materials, several factors can alter the crazing process (initiation, growth, and failure). The first is chain orientation. Block copolymers self-assemble into periodic nanoscale structures (sphere−bcc, cylinder−hexagonal, or lamellae).[16] Within these domains, chain conformations are in a perturbed state, not random Gaussian coils,[17] and the orientation of these stretched chains relative to that of applied stress can alter the crazing process. This effect of chain orientation has been observed previously for homopolymers.[18,19] The second factor is incompatibility. Most block copolymers (BCPs) consist of incompatible blocks. In crazing, matrix molecules are drawn to form a dense region of microfibrils which are 5−20 nm in diameter. Therefore, the incompatibility of segments in a block copolymer will impact the morphology of the craze fibril and/or the energy required for craze drawing. The last factor is the difference in mechanical properties among blocks. Will crazing be dictated by composite properties, or will it be confined to a single microdomain as in rubber−glass BCPs? In this paper, we present experimental results and a qualitative discussion of these factors, including the first evidence for the effect of nanoscale surface defects on the crazing process.

To understand the effect of BCP microstructure on crazing, we use symmetric polystyrene-*b*-poly(2-vinylpyridine) (PS-*b*-P2VP) as a model material. Because of the strong Flory interaction parameter between the two individual blocks and their relative interaction with air/substrate, thin films of this BCP can self-assemble into well-aligned one-dimensional lamellar domains parallel to the substrate (silicon oxide) solely by surface energetics.[20,21] This alignment helps to ensure that all chains have the same orientation relative to applied tensile stress and provides a model geometry for initial data analysis and interpretation. In addition to chain orientation, symmetric BCP thin films are known to form surface terraces (islands or holes) spontaneously due to a mismatch between the total film thickness and the molecular-defined lamellar spacing,[22,23] L_0 (Figure 1). These nanoscale "surface defects" are expected to alter local stress field and affect the microscopic crazing process. Finally, PS-*b*-P2VP is a model choice for this study due to the similar mechanical properties for each block (glass transition temperature, crazing stress, entanglement molecular weight, and elastic modulus).[24−26] These attributes allow us to focus on two primary effects: the effect of ordered microstructure and the effect of surface terraces on crazing (initiation, growth, and failure) in thin glassy polymer films. We find that the ordered lamellar microstructure results in slower craze growth rate and a larger ratio of craze depth to film thickness in the micronecking process. Additionally, surface terracing not only alters the craze initiation strain but also significantly decreases the failure strain of the thin films.

In the following sections, we describe our experimental methodology, present our results and relevant discussions, and summarize the main points of this paper. The overall flow of the paper follows the process of

* To whom correspondence should be addressed. E-mail: crosby@mail.pse.umass.edu.

10.1021/ma051716n CCC: $30.25
Published on Web 10/13/2005

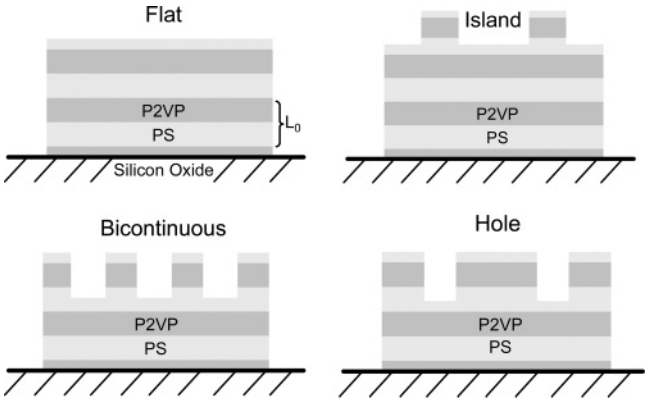

Figure 1. Surface morphologies of flat, island, bicontinuous, and hole on annealed symmetric diblock copolymer thin films (L_0: lamellae spacing).

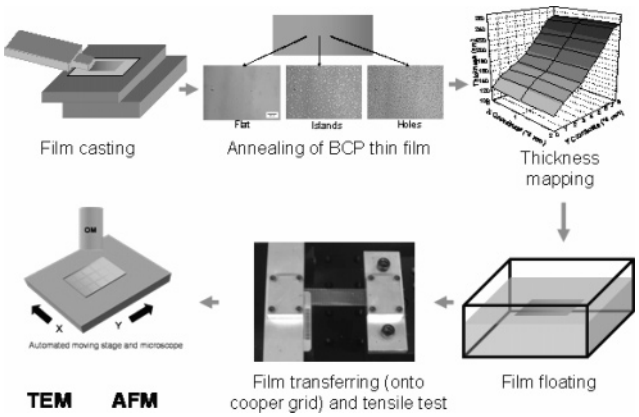

Figure 2. Summary of sample preparation, testing and craze characterization.

crazing: craze initiation, craze growth, and craze failure.

Experiment

Materials. PS-*b*-P2VP is obtained from Polymer Source Inc. The M_n of PS block is 57K, M_n of P2VP block is 57K, and PDI of PS-*b*-P2VP is 1.02. As a control, we compare crazing in PS-*b*-P2VP to crazing in homopolymer PS thin films. The PS is obtained from Polymer Source Inc. with a $M_n = 126$K and PDI = 1.02. Thin films of polystyrene are cast from 5.5 wt % toluene (Fisher-Scientific) solution, and PS-*b*-P2VP thin films are cast from 4.5 wt % toluene solution.

Combinatorial Methods. Total film thickness is expected to play a role in the crazing process of PS-*b*-P2VP.[27,28] Most directly, the total film thickness relative to the lamellar spacing (h/L_0) controls the number of lamellae available to contribute to crazing and dictates the type of the film surface morphology.[21−23] For example, if h/L_0 equals ($n + 0.5$), where n is a positive integer, then a flat surface (without terracing) can be obtained. If h/L_0 does not equal ($n + 0.5$), then surface terraces will decorate the thin film surface. The height of these terraces is controlled by L_0. To efficiently quantify the effect of all surface morphologies on crazing, we use a gradient-based combinatorial sample design. Specifically, our samples will consist of a thin film with a continuous gradient of film thickness in one direction. With this sample design, all surface morphologies are prepared in one library at one time. We divide grids of the whole library of PS-*b*-P2VP into three categories: flat surface without any terraces (BCP_F), surface partially covered by terraces (BCP_P), and surface completely covered by terraces (BCP_C). This library ensures that all samples are prepared, processed, and tested at the same time, thus providing experimental consistency. One library can have up to 138 samples (grids). Excluding grids with defects, there are 60 grids of BCP_C, 30 grids of BCP_F, and 30 grids of BCP_P. Additionally, three libraries are prepared and tested to confirm the results. The responses of all "samples" are averaged for the data points presented in Figures 4, 5, 7, and 12.

To accompany the increased efficiency in sample preparation, we have also developed a high-throughput method to collect optical microscopy images and perform subsequent analysis through a program written in the National Instrument's LabView environment. This image analysis routine standardizes our measurement process of craze morphology and minimizes error introduced by human interpretation.

Craze Characterization and Sample Preparation. To quantify the crazing process for polymer thin films, we use a well-established copper grid technique.[3] In short, this process involves floating and transferring a polymer film onto a copper grid substrate and subsequently straining the copper grid uniaxially. The copper grid strain is transferred to the polymer film, and because of the low yield strain and plasticity of annealed copper, the copper grid can maintain the applied strain after the sample is unloaded. Upon unloading at different applied strains, atomic force microscopy (AFM), optical microscopy (OM), and transmission electron microscopy (TEM) are then used to characterize the resultant crazes.

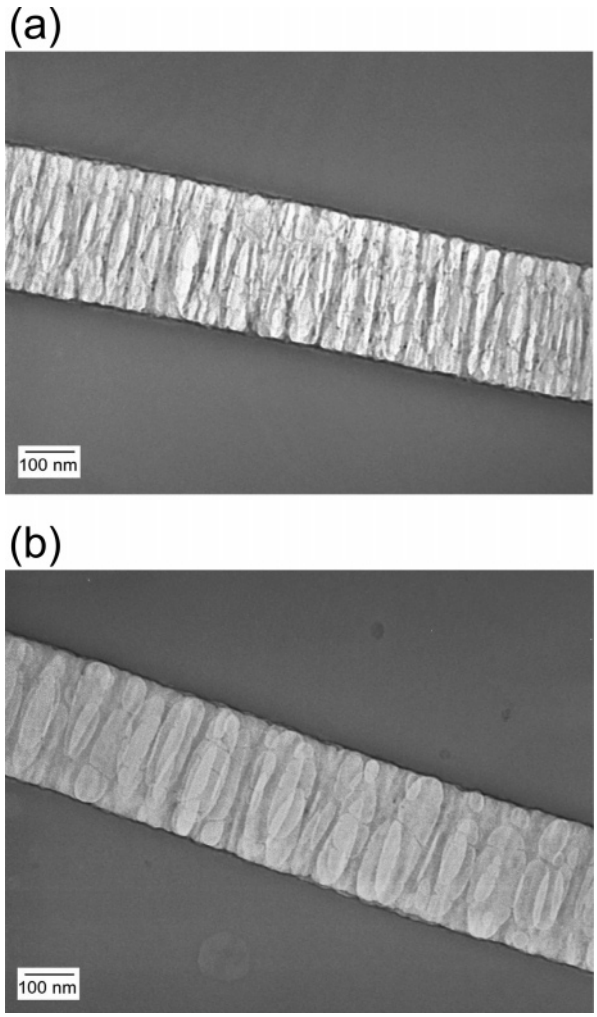

Figure 3. TEM images of fibril morphology in crazed regions of (a) PS and (b) PS-*b*-P2VP (film thickness is 244 nm; strain is 1.5%).

The processes of sample preparation, testing, and characterization are summarized in Figure 2. We begin by flow coating a thickness gradient thin film[29] on a silicon substrate with a thick silicon oxide layer (350 nm). The substrate is treated by acetone, toluene, and UV ozone prior to film casting. For flow coating, a volume of 0.1 mL dilute polymer solution is deposited under the flow coater razor blade, and then a

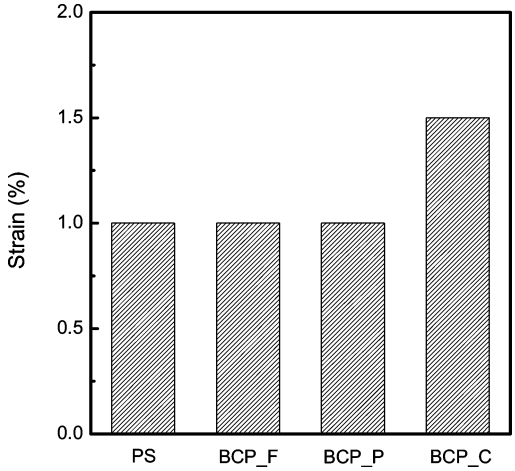

Figure 4. Craze initiation strain for PS, BCP_F, BCP_P, and BCP_C.

moving stage moves at a fixed acceleration to create a thickness gradient thin film. A thickness range of 130−250 nm can be obtained by controlling the acceleration of the moving stage and the height between the razor blade and substrate. For block copolymer thin films, the cast film is annealed at 180 °C under vacuum for 72 h. After annealing, periodic transitions of the surface morphology (flat to islands to holes) are observed along the thickness gradient direction. To quantify film thickness throughout the library, we make discrete and equally spaced thickness measurements by interferometry (Filmetrics) and interpolate a thickness map.

After mapping the film thickness, we float the film on water (for PS film) or 5 vol % aqueous hydrofluoric acid solution (for PS-*b*-P2VP film). Note that two edges of the film are removed during floating to avoid edge effects where irregular gradients in thin film thickness are observed. After floating block copolymer thin films, we extract hydrofluoric acid solution and replace with 0.2 M sodium hydroxide solution until the pH is larger than 10. This process removes the coordinated hydrofluoric acid ions in the P2VP segments of the BCP thin film. After this removal, we dilute the sodium hydroxide solution with water until the pH is equal to 7 and transfer the film onto a copper grid precoated by P2VP (for PS-*b*-P2VP film) or PS (for PS film) homopolymer. The film on the copper grid is dried for 12 h and then exposed to tetrahydrofuran (for PS-*b*-P2VP film) or toluene (for PS film) vapor to remove wrinkles and increase adhesion between the copper grid and the film. After exposure, the film is dried again for 24 h.

A custom-built, automated strain stage is used to apply fixed strain to the copper grid samples at a strain rate of 2.3×10^{-4}. For multiple strain experiments, we wait 10 min for crazes to reach equilibrium before unloading the copper grid.

To characterize the crazes at predefined strain, the copper grid is unloaded and fixed to a glass slide by tape. Optical microscopy images are taken for every grid square under bright and dark fields in an automated manner. Dark field enhances the contrast between the craze and the matrix, thus facilitating subsequent image analysis. Image analysis is performed in an automated, objective manner to obtain the number of crazes and area fraction occupied by crazes of each grid in the whole library.

To characterize certain morphological aspects of the crazes, AFM and TEM are used. For AFM, the strained copper grid is fixed to a glass slide by tape. To perform AFM on a film suspended by a copper grid, we scan the crazed regions close to the edge of the grid bars to prevent excess deflection. A similar technique has been previously described.[30] For TEM, we use a razor blade to cut a section from the copper grid. This section is then directly mounted into the TEM sample holder. Images are taken by a JEOL 2000FX under 200 keV acceleration voltage.

Results and Discussion

Craze vs Shear Deformation Zone. Crazing and shear yielding are both possible local deformation processes for glassy amorphous polymers.[31] Polymers with high entanglement molecular weight or low density of entanglements tend to craze, while polymers with low entanglement molecular weight or high density of entanglements tend to shear yield.[32,33] Since the entanglement molecular weight for chains in lamellar domains could be different compared to the chains in bulk state of homopolymers, we use TEM to characterize the deformation zones in both PS-*b*-P2VP and PS films. The deformation bands in all grids of PS and PS-*b*-P2VP with different film thickness (135−245 nm) consist of dense arrays of fibrils, which are characteristic of traditional crazes. These images show that fibril morphology (diameter and density) does not change over this thickness range, but some differences exist between PS and the BCP. The density of fibrils in the crazed region of PS is higher than that of PS-*b*-P2VP (Figure 3), thus implying that the fibril extension ratio of PS-*b*-P2VP is larger compared with PS. The details about fibril extension ratio are given below in a section on craze growth and micronecking. We also find that the fibril morphology in the flat region is the same as that in the hole and island domains; therefore, surface terracing does not cause any changes in fibril morphology.

Craze Initiation. Crazes are nucleated from surface defects or inclusions. According to accepted theories,[1,34] these regions lead to stress concentration and the existence of a hydrostatic stress which leads to local yielding, cavitation, and subsequent nucleation of a craze. For our PS thin films, most crazes are initiated at the edge of the copper grid where the most significant defects reside. Similarly, most crazes in our PS-*b*-P2VP films (terraced or flat surface) also initiate from the edge of the grid, but in a few cases, surface terraces are found to serve as craze initiation sites. In these cases, the islands or holes are isolated and large and serve as a significant defect in the thin film structure. This observation is interesting in light of previous research on the initiation of crazes in rubber-toughen polystyrene. For these materials, crazes are initiated from spherical particles that are at least 1 μm in diameter.[35] The surface terraces of our BCP have lateral dimensions over 5 μm, but the height of these defects is only on the order of 50 nm or one lamellae period. This impact demonstrates that defects with nanoscale dimensions can significantly alter the continuum stress field. As we discuss below, this stress alteration impacts not only craze initiation but also failure of the material.

Although the nucleation of crazes by surface terraces is not a dominating effect in our samples, we do observe an alteration in the initiation process by the presence of surface terraces. Specifically, we find that the strain at which crazes are initiated is larger for PS-*b*-P2VP films that are completely covered with surface terraces (BCP_C in Figure 4). (Note that craze initiation strain for BCP_F, BCP_P, and BCP_C is defined as over 50% grids of the category having at least one craze.) This increase in initiation strain is not large, but it is statistically significant. Because of the combinatorial design of our sample library, we can confidently say that the initiation strain in flat, nonterraced regions of our structured BCP film is not altered; therefore, this delayed initiation is not a material difference but one

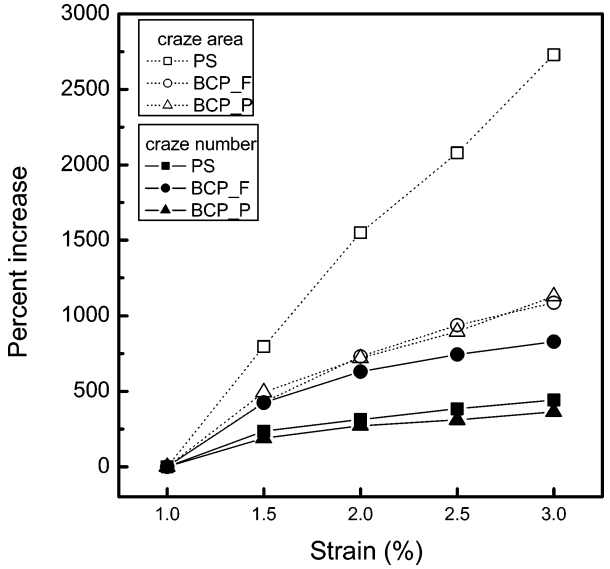

Figure 5. Percent increase of the number of crazes (solid symbol) and area fraction occupied by crazes (hollow symbol) per grid of PS, BCP_F, and BCP_P as a function of applied tensile strain. Data points for PS are compiled averages of over 120 and 30 grids for BCP_F and BCP_P, respectively.

dictated by the surface geometry. In fact, PS-*b*-P2VP has the same initiation mechanism as PS based on a plot—the percent increase of the number of crazes as a function of different strains (Figure 5). In this plot, BCP_F, BCP_P, and PS all have similar trends. Since BCP_C fails at 2% strain, it is not included in Figure 5. We also know that this alteration in strain is not a consequence of changing film thickness. For PS thin films with thickness varying from 135 to 245 nm, no deviation in the initiation strain (1%) is observed as a function of thickness.

Craze Growth. According to previous research and current models,[2,33,34] crazes grow in length by a meniscus instability and in thickness by drawing polymer chains from the unyielded matrix into the craze (surface drawing). As strain increases, crazes become wider and longer. In PS, this process produces long, straight, stable crazes. To compare craze growth in PS to our BCP films, we define a rate (R_c) of craze growth as the increase of normalized area fraction (A_f) per unit strain. R_c will be dependent on strain rate, temperature, and other experimental conditions.

$$R_c = \frac{\partial A_f}{\partial \epsilon}$$

$$A_f = \frac{\text{area fraction occupied by crazes per grid}}{\text{number of crazes per grid}} \times 100$$

$$\epsilon = \text{tensile strain}$$

A_f is also equivalent to the average area fraction of one craze in one grid. Since the percent increase of the number of crazes in a given square of PS does not change significantly with applied strain compared with percent increase of area fraction occupied by crazes in a given square of PS (Figure 5), A_f is dominated by craze growth, not nucleation. For our PS libraries, we observe that thickness has little to no effect on A_f within the thickness range of 135−245 nm (Figure 6). This observation is expected according to current models on craze growth.[27,28] (Note that each data point in Figure 6 is the average result from six grids with the same thickness.)

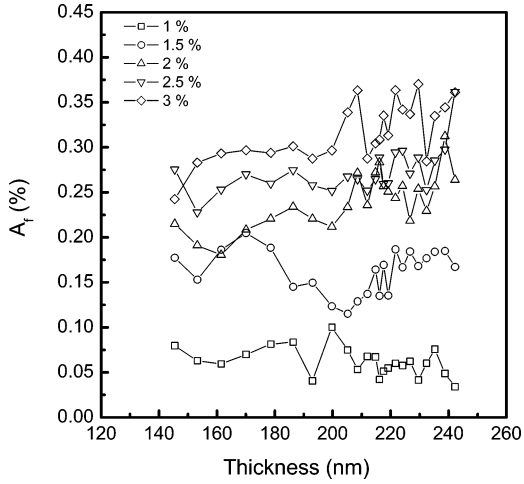

Figure 6. Normalized area fraction (A_f) as a function of film thickness of PS.

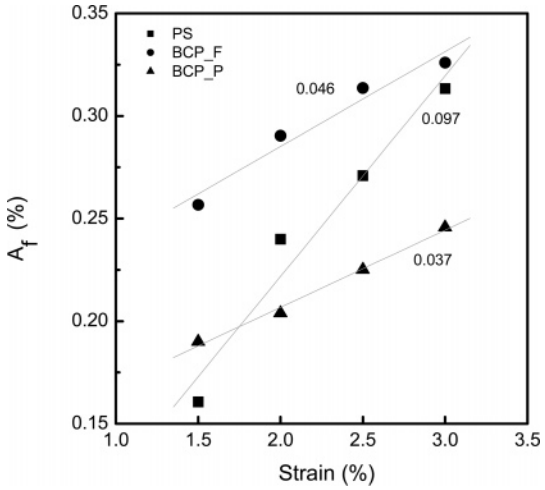

Figure 7. Plot of normalized area fraction (A_f) as a function of tensile strain for PS, BCP_F, and BCP_P. The numbers are the slopes of linear fitting lines. Data points for PS are compiled averages of over 120 and 30 grids for BCP_F and BCP_P, respectively.

The relationship between A_f and strain is linear for PS, BCP_F, and BCP_P (Figure 7), and the slope is the craze growth rate, R_c, as defined above. This slope is equivalent to the average growing extent of one craze in one grid per strain, and we only consider this growth at applied strain ≥1.5 after most crazes have initiated. Since over 50% of the grids for BCP_C fail at 2% strain, we do not plot BCP_C in Figure 7. Crazing is an energetic process where the applied strain energy drives the development of crazes. Therefore, Figure 7 compares the use of applied strain energy in different materials. BCP_F and BCP_P have very similar slopes, and this suggests that a minority coverage of surface terraces has little to no effect on the rate of craze growth. On the other hand, PS and BCP_F have very different rates of craze growth. This observation implies that craze growth in PS-*b*-P2VP lamellar films is more energetically costly compared to PS. We attribute this energy difference to the fibril formation in PS-*b*-P2VP. To form fibrils in an aligned block copolymer film, chains need to rotate due to the direction of the applied stress field relative to the orientation of chains in their lamellar

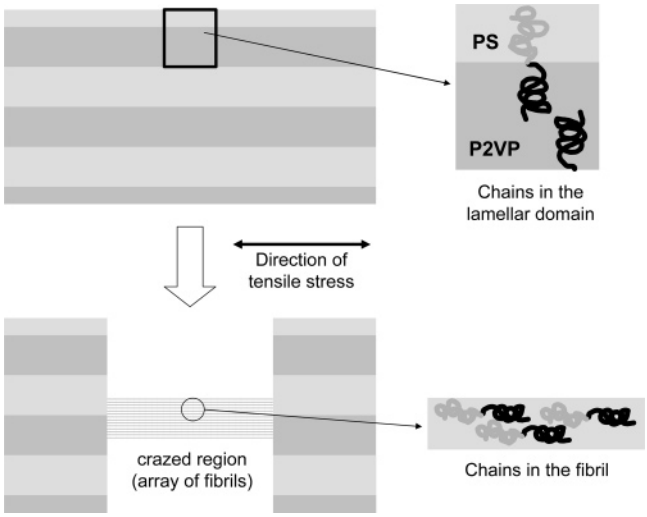

Figure 8. Chain conformation in the lamellar domain of symmetric diblock copolymer thin film before and after tensile load.

domains. Additionally, upon drawing into the craze fibrils, the two incompatible blocks are confined to fibrils that are 10−20 nm (Figure 8). Both of these two processes require additional energy; therefore, the growth of a craze per unit strain in PS-*b*-P2VP requires more energy and will proceed at a slower rate. This effect can be summarized in the form of a relationship:

$$E_{\mathrm{app}} = E_{\mathrm{c}} + E_{\mathrm{rot}} + E_{\mathrm{int}}$$

$$\frac{\partial E_{\mathrm{app}}}{\partial \epsilon} = \frac{\partial E_{\mathrm{c}}}{\partial \epsilon} + \frac{\partial E_{\mathrm{rot}}}{\partial \epsilon} + \frac{\partial E_{\mathrm{int}}}{\partial \epsilon}$$

where E_{app} is the applied strain energy, E_{c} is the energy of crazing (craze growth), E_{rot} is the energy of chain rotation, and E_{int} is the interaction energy of polymer chains in fibrils. On the basis of the result of Farrar and Kramer,[18] the surface stress for crazing is larger for preoriented chains perpendicular to the applied tensile direction compared with the case of chains parallel to the applied tensile direction. This result implies that fibril formation for the perpendicular case takes more energy compared to the parallel case. For homopolymers where chains are randomly arranged, $\partial E_{\mathrm{rot}}/\partial \epsilon$ is much less than that of our BCP thin films with oriented chains perpendicular to tensile direction. Additionally, because of incompatibility between two individual blocks, $\partial E_{\mathrm{int}}/\partial \epsilon$ of BCP is much larger than that of PS. Therefore, if $\partial E_{\mathrm{rot}}/\partial \epsilon$ and $\partial E_{\mathrm{int}}/\partial \epsilon$ are larger for BCP and the $\partial E_{\mathrm{app}}/\partial \epsilon$ is the same for both BCP and PS since their moduli are nearly identical, then $\partial E_{\mathrm{c}}/\partial \epsilon$ will be less for the BCP, as observed in Figure 7.

In addition to growing in length and width, crazes in thin films also experience a micronecking process in the thickness direction. One quantity that describes this micronecking is the ratio of craze depth to total film thickness. Yang et al.[36] reported the ratio of depth of craze in PS to total film thickness is a constant, equal to 0.35. Similarly, Crosby et al.[30] used a combinatorial method to investigate microneckong phenomenon in PS and measured statistically a ratio of 0.37. In our measurements on PS, we also measured a ratio of 0.37, but for PS-*b*-P2VP the craze depth ratio equals 0.47. This ratio is maintained not only in flat regions but also as crazes pass through island and hole domains (Figure

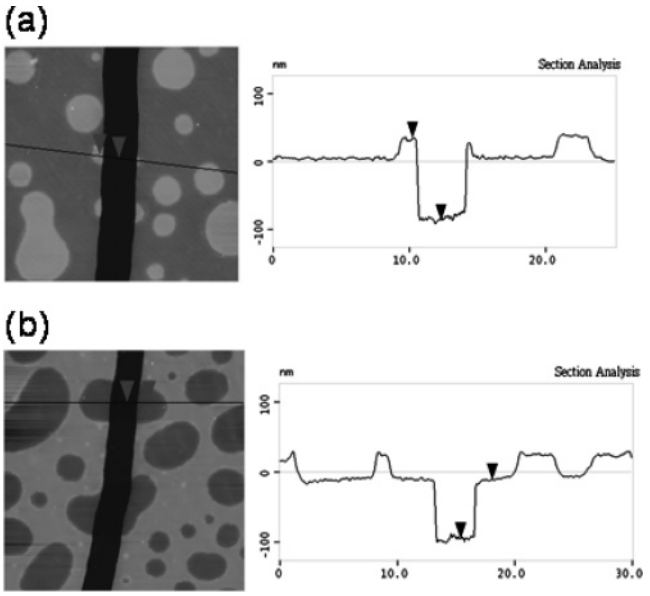

Figure 9. AFM images (a) craze-in-island and (b) craze-in-hole. The image size is 30 μm × 30 μm. Film thickness is 244 nm in island regions, 136 nm in hole regions, and 190 nm in flat regions. Applied tensile strain is 1.5%.

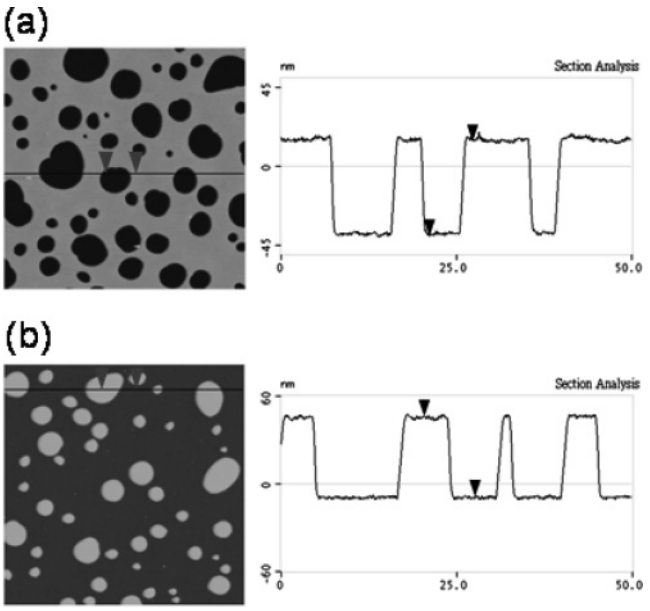

Figure 10. AFM images of (a) island domains and (b) hole domains on annealed PS-*b*-P2VP thin film cast on silicon substrate with thick oxidized layer (350 nm). The height of islands and depth of holes are both 54 nm obtained from section analysis. The image size is 50 μm × 50 μm. Film thickness is 244 nm in island regions, 136 nm in hole regions, and 190 nm in flat regions.

9). In these terraced regions, the constant ratio is calculated by using the exact local thickness of $L_0(n + 0.5)$, where L_0 is the lamellae spacing and n is the number of lamellae. L_0 is measured by the height of islands and depth of holes (Figure 10). The depth of the craze is measured directly from AFM section analysis.

The craze depth ratio of 0.47 for all crazes in PS-*b*-P2VP compared to 0.37 for PS suggests that this ratio is material dependent. Micronecking requires the extension of craze fibrils from the uncrazed surface to the surface depth of craze section. Therefore, the depth-to-thickness ratio is related to the fibril extension ratio. Larger depth-to-thickness ratio implies a larger fibril

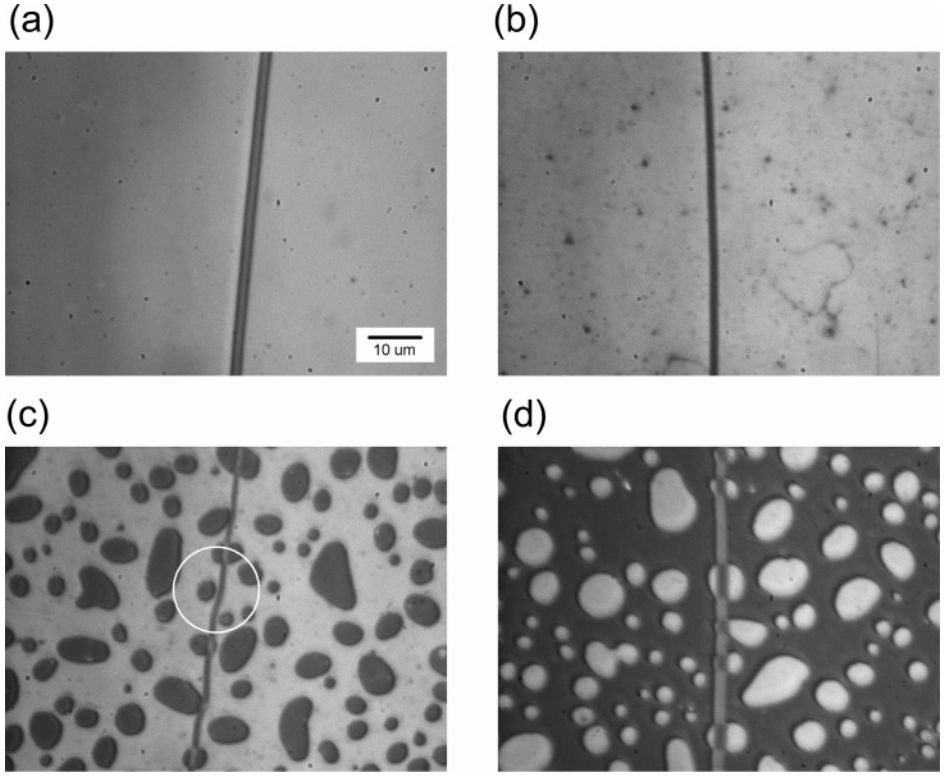

Figure 11. Optical microscopy images of crazes on (a) PS and (b) PS-*b*-P2VP with flat surface, (c) with island domains (the circled area emphasized the evading of the craze), and (d) with hole domains.

extension ratio.[37] On the basis of our measurements, PS-*b*-P2VP has a larger depth-to-thickness ratio, so it has a larger fibril extension ratio compared to PS. This result is also consistent with our observations of the less dense fibril morphology compared to PS in TEM micrographs. Since the film thickness in a PS-*b*-P2VP crazed region is thinner (due to high depth-to-thickness ratio) than that in PS, there are less fibrils in the crazed region compared with PS. We attribute the higher fibril extension ratio to the chain orientation in lamellar domains, similar to the observations of Creton and Kramer.[38] In their experiments, Creton and Kramer measured craze morphology in a film of poly(2-vinylpyridine)-*b*-polystyrene-*b*-poly(2-vinylpyridine) with a lamellar morphology. They found that the fibril extension ratio is 5.7 for chains perpendicular to tensile direction and 4.4 for chains parallel to tensile direction. From these results, they calculated the chain extension ratio of 1.2 in lamellar domains before deformation. This increase is consistent with our observations of the increased micronecking ratio.

Although surface terraces do not play a dominant role in altering the craze growth process compared to inherent material properties such as the fibril extension ratio and incompatibility between blocks, surface terraces can alter the local stress distribution. This stress change is observed to alter the path of craze propagation. In the absence of surface terraces, such as films of PS and PS-*b*-P2VP with flat surfaces, crazes are straight, narrow bands (Figure 11a,b). Crazes in PS-*b*-P2VP with terraced surfaces are slightly sinuous (Figure 11c,d). We attribute this altered propagation path to the influence of local stress fields. For example, because of the increased local thickness within an island domain, the local stress is lower compared to surrounding regions. Therefore, as a craze approaches an island domain, the preferred path of propagation is around the island domain where the stress and energy are higher. This diversion of crazes around island domains is also dependent upon the deflection angle. On the contrary, the stress near a surface hole is greater than surrounding regions, so crazes are "attracted" to hole domains. They tend to pass through the holes, not evade them. Regardless of the direct action, these observations point to the impact of nanoscale defects on failure mechanisms in thin polymer films. Even though the island and hole domains only have a height of 54 nm, they create local stress fields that significantly alter the onset, propagation, and failure of local crazes.

Craze Failure. It is known that the failure of crazed materials is caused by fibril breakdown at the interface between the crazed region and matrix during the surface drawing process.[7,33] Fibril breakdown is largely due to the existence of stress concentrating defects, such as dust particles or intrinsic weak spots (e.g., chain ends) which cannot support stress. For PS and flat regions of PS-*b*-P2VP, these mechanisms persist, and the failure strain in both cases is measured as 7% strain. As surface terraces appear in the PS-*b*-P2VP films, the failure strain decreases with increasing coverage of these nanoscale surface defects. (Note that failure strain of crazes is defined as over 50% grids of a given morphology having failed.) The reason for the early failure is the increased occurrence or high probability for crazes to propagate into island or hole domains. Both island and hole domains are sudden changes in the local film thickness. Therefore, at their boundaries, a large stress gradient or stress concentration is generated. Consequently, these domains serve as stress concentration points, similar to dust particles responsible for conventional fibril breakdown. Accordingly, this mechanism is independent of materials, and nanoscale surface defects in other crazing polymers are expected to act in a similar manner. Figure 12 shows the failure

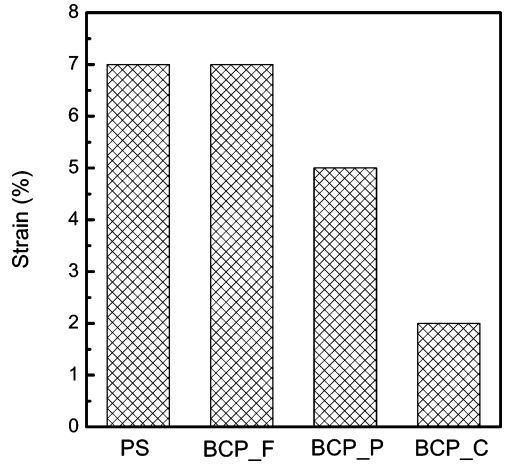

Figure 12. Failure strain for PS, BCP_F, BCP_P, and BCP_C.

strain among PS and PS-*b*-P2VP with different surface morphologies. For BCP_C, the effect of surface terraces is quite dramatic since craze initiation is delayed and failure is promoted at early strain. Overall, these data truly points to the importance of surface defects at the nanoscale on impacting the strength of polymer thin films.

Conclusion

Surface terraces that self-assemble on the surface of BCP thin films alter the initiation, growth, and failure of crazes in these materials. Specifically, they slightly delay the initiation of crazes, alter the path of crazes, and ultimately decrease the failure strain by more than 70%. While these effects are significant, we also find that surface terraces do not have any influence on fibril morphology, craze growth rate, and the depth-to-thickness ratio in the micronecking process. These results not only show how crazing in thin films can be altered through self-assembled surface microstructures but also demonstrate the importance of "surface defects" in the overall integrity of polymer thin films and coatings.

Beyond surface terraces, the microstructure of aligned, lamellar PS-*b*-P2VP alters the crazing process compared to homopolymer PS films. We find by TEM craze morphology analysis and AFM quantification of micronecking that the lamellar PS-*b*-P2VP films have a larger fibril extension ratio compared to PS. This change in fibril extension ratio also causes the depth-to-thickness ratio for micronecking to be 0.47 for block copolymer compared to 0.37 for PS. The craze growth rate in PS-*b*-P2VP is also smaller compared to PS. This difference is associated with the increased energy required to form fibrils in the aligned BCP film due to the rotation of chains and confinement of two incompatible blocks within single fibrils. Overall, these results demonstrate the importance of nanoscale morphologies on the crazing process and point to new directions for understanding the fundamental mechanisms for crazing in advanced materials.

Acknowledgment. Funding for this project is provided by the NSF-MRSEC at the University of Massachusetts and the American Chemical Society Petroleum Research Fund.

References and Notes

(1) Argon, A. S.; Hannoosh, J. G. *Philos. Mag.* **1977**, *36*, 1195−1216.
(2) Argon, A. S.; Salama, M. M. *Philos. Mag.* **1977**, *36*, 1217−1234.
(3) Lauterwasser, B. D.; Kramer, E. J. *Philos. Mag. A* **1979**, *39*, 469−495.
(4) Donald, A. M.; Kramer, E. J.; Bubeck, R. A. *J. Polym. Sci., Part B: Polym. Phys.* **1982**, *20*, 1129−1141.
(5) Donald, A. M.; Kramer, E. J. *J. Polym. Sci., Part B: Polym. Phys.* **1982**, *20*, 899−909.
(6) Michler, G. H. *Colloid Polym. Sci.* **1986**, *264*, 522−532.
(7) Yang, A. C. M.; Kramer, E. J.; Kuo, C. C.; Phoenix, S. L. *Macromolecules* **1986**, *19*, 2010−2019.
(8) Krupenkin, T. N.; Fredrickson, G. H. *Macromolecules* **1999**, *32*, 5036−5045.
(9) Rottler, J.; Robbins, M. O. *Phys. Rev. E* **2003**, 68.
(10) Schwier, C. E.; Argon, A. S.; Cohen, R. E. *Polymer* **1985**, *26*, 1985−1993.
(11) Schwier, C. E.; Argon, A. S.; Cohen, R. E. *Philos. Mag. A* **1985**, *52*, 581−603.
(12) Honeker, C. C.; Thomas, E. L. *Chem. Mater.* **1996**, *8*, 1702−1714.
(13) Weidisch, R.; Ensslen, M.; Michler, G. H.; Fischer, H. *Macromolecules* **1999**, *32*, 5375−5382.
(14) Weidisch, R.; Ensslen, M.; Michler, G. H.; Arnold, M.; Budde, H.; Horing, S. *Macromolecules* **2001**, *34*, 2528−2535.
(15) Ryu, C. Y.; Ruokolainen, J.; Fredrickson, G. H.; Kramer, E. J.; Hahn, S. F. *Macromolecules* **2002**, *35*, 2157−2166.
(16) Bates, F. S.; Fredrickson, G. H. *Annu. Rev. Phys. Chem.* **1990**, *41*, 525−557.
(17) Hasegawa, H.; Hashimoto, T.; Kawai, H.; Lodge, T. P.; Amis, E. J.; Glinka, C. J.; Han, C. C. *Macromolecules* **1985**, *18*, 67−78.
(18) Farrar, N. R.; Kramer, E. J. *Polymer* **1981**, *22*, 691−698.
(19) Maestrini, C.; Kramer, E. J. *Polymer* **1991**, *32*, 609−618.
(20) Coulon, G.; Russell, T. P.; Deline, V. R.; Green, P. F. *Macromolecules* **1989**, *22*, 2581−2589.
(21) Fasolka, M. J.; Mayes, A. M. *Annu. Rev. Mater. Res.* **2001**, *31*, 323−355.
(22) Russell, T. P.; Coulon, G.; Deline, V. R.; Miller, D. C. *Macromolecules* **1989**, *22*, 4600−4606.
(23) Cai, Z. H.; Huang, K. G.; Montano, P. A.; Russell, T. P.; Bai, J. M.; Zajac, G. W. *J. Chem. Phys.* **1993**, *98*, 2376−2386.
(24) Creton, C.; Kramer, E. J.; Hadziioannou, G. *Macromolecules* **1991**, *24*, 1846−1853.
(25) Washiyama, J.; Creton, C.; Kramer, E. J. *Macromolecules* **1992**, *25*, 4751−4758.
(26) Bucknall, C. B.; Cote, F. F. P.; Partridge, I. K. *J. Mater. Sci.* **1986**, *21*, 301−306.
(27) Donald, A. M.; Chan, T.; Kramer, E. J. *J. Mater. Sci.* **1981**, *16*, 669−675.
(28) Chan, T.; Donald, A. M.; Kramer, E. J. *J. Mater. Sci.* **1981**, *16*, 676−686.
(29) Meredith, J. C.; Smith, A. P.; Karim, A.; Amis, E. J. *Macromolecules* **2000**, *33*, 9747−9756.
(30) Crosby, A. J.; Fasolka, M. J.; Beers, K. L. *Macromolecules* **2004**, *37*, 9968−9974.
(31) Si, L.; Massa, M. V.; Dalnoki-Veress, K.; Brown, H. R.; Jones, R. A. L. *Phys. Rev. Lett.* **2005**, 94.
(32) Donald, A. M.; Kramer, E. J. *J. Mater. Sci.* **1982**, *17*, 1871−1879.
(33) Kramer, E. J.; Berger, L. L. *Adv. Polym. Sci.* **1990**, *91/91*, 2−68.
(34) Kramer, E. J. *Adv. Polym. Sci.* **1983**, *52−3*, 1−56.
(35) Donald, A. M.; Kramer, E. J. *J. Appl. Polym. Sci.* **1982**, *27*, 3729−3741.
(36) Yang, A. C. M.; Kunz, M. S.; Logan, J. A. *Macromolecules* **1993**, *26*, 1767−1773.
(37) Lin, J. H.; Yang, A. C. M. *Macromolecules* **2001**, *34*, 3698−3705.
(38) Creton, C.; Kramer, E. J.; Hadziioannou, G. *Colloid Polym. Sci.* **1992**, *270*, 399−404.

MA051716N